

Passive coupling of membrane tension and cell volume during active response of cells to osmosis

Chloé Roffay^a, Guillaume Molinard^a, Kyoohyun Kim (김규현)^{b,c}, Marta Urbanska^{b,c}, Virginia Andrade^{d,e}, Victoria Barbarasa^a, Paulina Nowak^{a,f}, Vincent Mercier^a, José García-Calvo^g, Stefan Matile^{g,h}, Robbie Loewith^{f,h}, Arnaud Echard^d, Jochen Guck^{b,c}, Martin Lenz^{i,j}, and Aurélien Roux^{a,h,1}

^aDepartment of Biochemistry, University of Geneva, CH-1211 Geneva, Switzerland; ^bMax Planck Institute for the Science of Light, DE-91058 Erlangen, Germany; ^cBiotechnology Center, Technische Universität Dresden, D-01307 Dresden, Germany; ^dMembrane Traffic and Cell Division Laboratory, Institut Pasteur, Université de Paris, CNRS UMR3691, F-75015 Paris, France; ^eCollège Doctoral, Sorbonne Université, F-75005 Paris, France; ^fDepartment of Molecular Biology, University of Geneva, CH-1211 Geneva, Switzerland; ^gDepartment of Organic Chemistry, University of Geneva, CH-1211 Geneva, Switzerland; ^hNational Centre of Competence in Research Chemical Biology, University of Geneva, CH-1211 Geneva, Switzerland; ⁱLaboratory of Theoretical Physics and Statistical Models, Université Paris-Saclay, CNRS, F-91405 Orsay, France; and ^jPhysique et Mécanique des Milieux Hétérogènes UMR 7636, CNRS, École Supérieure de Physique et de Chimie Industrielles de la Ville de Paris, Paris Sciences & Lettres University, Sorbonne Université, Université de Paris, F-75005 Paris, France

Edited by Pietro De Camilli, Yale University and HHMI, New Haven, CT, and approved October 7, 2021 (received for review February 17, 2021)

During osmotic changes of their environment, cells actively regulate their volume and plasma membrane tension that can passively change through osmosis. How tension and volume are coupled during osmotic adaptation remains unknown, as their quantitative characterization is lacking. Here, we performed dynamic membrane tension and cell volume measurements during osmotic shocks. During the first few seconds following the shock, cell volume varied to equilibrate osmotic pressures inside and outside the cell, and membrane tension dynamically followed these changes. A theoretical model based on the passive, reversible unfolding of the membrane as it detaches from the actin cortex during volume increase quantitatively describes our data. After the initial response, tension and volume recovered from hypoosmotic shocks but not from hyperosmotic shocks. Using a fluorescent membrane tension probe (fluorescent lipid tension reporter [Flipper-TR]), we investigated the coupling between tension and volume during these asymmetric recoveries. Caveolae depletion and pharmacological inhibition of ion transporters and channels, mTORCs, and the cytoskeleton all affected tension and volume responses. Treatments targeting mTORC2 and specific downstream effectors caused identical changes to both tension and volume responses, their coupling remaining the same. This supports that the coupling of tension and volume responses to osmotic shocks is primarily regulated by mTORC2.

plasma membrane tension | cell volume | flipper-TR | osmotic shocks | mechanobiology

Lipid membranes are self-assembled viscoelastic bilayers separating cells and their organelles from their environment (1). They are easy to bend but resistant to stretching: Their lysis tension—the tension at which they break—is high, in the range of a few millinewtons per meter (2). This high value protects cells against lysis upon processes that stretch the cell membrane, but it still cannot protect from the huge stretch generated by hypotonic shocks (3). Plasma membrane tension arises from the combined contributions of osmotic pressure, in-plane tension, and cytoskeletal forces (4). The cytoskeleton is intimately linked to all processes regulating membrane tension, in particular cell volume regulation (5). For example, hypotonic shocks not only are responsible for increasing membrane tension (6, 7) but also induce the degradation of vimentin (8) and a reorganization of actin filaments (9, 10), without strongly affecting microtubules (8). The cytoskeleton regulates membrane tension by setting its value through active force generation and by establishing a membrane reservoir that buffers acute changes in tension (11). This membrane reservoir is stored around protruding actin-based structures such as ruffles, filopodia, and microvilli.

Part of this membrane reservoir is also stored in caveolae, which are plasma membrane invaginations formed by the

assembly of Cavin1-3 and Caveolin1-2, and their disassembly buffers membrane tension increase (6). Cell volume regulation during osmotic changes involves mechanosensitive ion transporters and channels (12, 13) regulated by membrane tension (14). How their activity is coupled to the cytoskeleton is under debate (15). They comprise volume-regulated anion channels (VRACs), sodium–hydrogen antiporters (NHEs), and Na–K–Cl cotransporters (NKCC1). VRACs are activated by hypotonic stress (16) and are unique in transporting small organic osmolytes—in particular, taurine—in addition to anions (17). NHEs inhibition prevents regulatory volume increase of cells (18). Cells have evolved to respond to changes in membrane tension and control its impact on many processes essential to cell life (19). The genetic response to an osmotic stress

Significance

Tension is the force-opposing stretch of lipid membranes. It controls cell functions involving membranes. Membranes rupture above a tension threshold, causing cell death if tension is not properly buffered. However, how cell membrane tension is quantitatively regulated is unknown because it is difficult to measure. Using a fluorescent membrane tension probe, we explored the coupling between membrane tension and cell volume changes during osmosis. This coupling is described by an equilibrium theory linking tension to folding and unfolding of the membrane. This coupling is nevertheless actively regulated by cell components such as the cytoskeleton, ion transporters, and mTOR pathways. Our results highlight that cell volume regulation and membrane tension homeostasis are independent from the regulation of their coupling.

Author contributions: C.R. and A.R. designed research; G.M. performed the tube pulling and PI experiments and C.R. and G.M. analyzed the data; K.K. performed the ODT measurements and analyzed the data; C.R. and V.B. performed the GFP transfected cells experiments and analyzed the data; M.U. performed the cell volume measurement on HL-60 using RT-DC and analyzed the data; P.N. performed the Western blot of mTORCs activities in various conditions; V.A. and A.E. generated the Cavin1-KO stable cell line; C.R. performed all other experiments and analysis; V.M., J.G.-C., S.M., R.L., and J.G. contributed new reagents/analytic tools; M.L. conducted the theory and fits to experiments; and C.R., M.L., and A.R. wrote the manuscript, with edits from all other coauthors.

The authors declare no competing interest.

This article is a PNAS Direct Submission.

This open access article is distributed under [Creative Commons Attribution-NonCommercial-NoDerivatives License 4.0 \(CC BY-NC-ND\)](https://creativecommons.org/licenses/by-nc-nd/4.0/).

¹To whom correspondence may be addressed. Email: aurelien.roux@unige.ch.

This article contains supporting information online at <https://www.pnas.org/lookup/suppl/doi:10.1073/pnas.2103228118/-DCSupplemental>.

Published November 16, 2021.

has been studied extensively. This pathway partly consists of activating genes involved in the synthesis or degradation of osmo-protectant molecules (such as glycerol in yeast and amino acids in mammalian cells) and their subsequent secretion (20, 21). However, the timescale of the genetic response to osmotic stress—on the order of tens of minutes—cannot account for the cell's immediate resistance to stretch (18, 21). The master regulator of plasma membrane tension is probably Target of Rapamycin Complex 2 (TORC2) (22) and its mammalian homolog mTORC2. TORC2 and mTORC2 are assembled around the kinase TOR (mTOR), which is also part of TORC1 and mTORC1. While TORC1 and mTORC1 are involved in cell volume regulation (23, 24), TORC2 and mTORC2 are involved in membrane tension regulation (7, 25, 26). Indeed, TORC2 signaling increases instantaneously upon membrane tension increase (27) as well as mTORC2 activity (7) and decreases upon tension loss (25). TORC2 regulates endocytosis through membrane tension (26), but also actin polymerization, as knockdown of mTORC2, but not mTORC1, prevents actin polymerization (28) and increases membrane tension (7). The increased tension could be linked to the role of cortical actin in folding the membrane into ruffles, controlling the size of the membrane area buffer (29).

Despite its undeniable importance, the mechanisms driving the regulation of membrane tension during osmotic shocks in relation to cell volume changes are still poorly understood. Qualitatively, membrane tension has been reported to decrease in response to hypertonic shocks (30, 31), while studies have reported that it either stays constant (31, 32) or increases (6, 30, 33) upon hypotonic shock. The relation between osmolarity and cell volume change is captured by the Ponder/Boyle/Vant'Hoff (PBVH) relation whereby cell volume changes until the osmotic pressure of its contents matches that of the extracellular medium (34). This relation involves an osmotically inactive volume (V_{OI}), which represents the minimum volume occupied by tightly packed cellular constituents at very high hypertonicity (23, 35, 36). However, while the PBVH relation describes the changes in cell volume in response to an osmotic shock, the membrane tension response to such shocks has never been quantitatively studied. In this study, we elucidate quantitatively the coupling between cell volume and membrane tension in single cells during osmotic shocks using time-resolved techniques.

Results

Cell Volume Change upon Osmotic Shock. We measured volume changes in HeLa Kyoto cells labeled with the plasma membrane probe CellMask and exposed to stepwise osmotic shocks (Fig. 1 *A* and *B* and *Materials and Methods*). Volumes were obtained by segmenting time-lapse three-dimensional (3D) confocal stacks of CellMask images. Imaging giant unilamellar vesicles (GUVs), we estimated the error of our volume quantification to be less than 5%, after all required corrections (*SI Appendix, Fig. S1A*). The average cell volume peaked at approximately 2.4 times the initial volume, a few seconds after a hypotonic shock (120 mOsm). It subsequently recovered, but only partially, leaving a 15% volume increase after 10 min (Fig. 1*C*). Weaker dilutions (50% and 25%) led to lower peaks (Fig. 1*C*). Cell porosity measured using propidium iodide (PI) in hypotonic medium was null (*SI Appendix, Fig. S1B*). Conversely, hypertonic shocks led to a rapid volume decrease within seconds, followed by a 10-min plateau. Cells were not porous (*SI Appendix, Fig. S1B*) and cell metabolism after 1 h in hypertonic buffer up to 900 mOsm was more than 60% (*SI Appendix, Fig. S1C*) and equal to 100% if cells were left to recover overnight in isotonic medium (*SI Appendix, Fig. S1D*). In the most extreme hypertonic conditions (3,500 mOsm), cell volume decreased by up to 90% (*SI Appendix, Fig. S1E and F*). Before the osmotic shocks, cell volume distributions were broad (Fig. 1*C*) while relative cell

volume changes were highly reproducible. Using an EGFP-LaminB1 stable cell line, we measured nuclei and cell volume changes and showed that cell volume changes were essentially due to cytoplasmic volume changes (*SI Appendix, Fig. S2*). To assess the robustness of the recovery dynamics, we performed cell volume measurements using a different cell type (HL-60/S4) using real-time deformability cytometry (RT-DC)—a high-throughput technique allowing for rapid characterization of thousands of cells (37) (*SI Appendix, Fig. S3A*). After applying the osmotic shocks to HL-60/S4 cells before loading them into RT-DC, we confirmed our previous observation: Cell volume in a hypotonic medium peaked and recovered while cell volume in a hypertonic medium abruptly and stably decreased (*SI Appendix, Fig. S3B and C*). However, the characteristic time of the recovery is probably cell type dependent and whether cells are adherent or not may impact this characteristic time (38). Our results show that the volume changes associated with osmotic shocks are rapid, with an asymmetric recovery, immediate for hypotonic shocks and very slow for hypertonic shocks. Based on these observations and previous results (25, 27), we hypothesize that the regulation of cell response to hypotonic shocks is distinct from the regulation of cell response to hypertonic shocks.

Membrane Tension Changes Are Coupled to Cell Volume Changes.

We then measured changes of membrane tension after osmotic shocks. When membrane tubes are pulled from the cell membrane using beads held with optical tweezers, the force required to statically hold the tube is a direct measurement of membrane tension. The distribution of tube forces before osmotic shock f_0 was broad: 27 ± 18 pN (Fig. 1*D*). Changes in the tube force upon osmotic shocks were fast (a few seconds) and below the temporal resolution of the cell volume acquisition (*SI Appendix, Fig. S3D and E*). Interestingly, changes of the tube force $(f - f_0)/f_0$ averaged over 10 s immediately following the shock were according to the intensity of the shocks (Fig. 1*D* and *SI Appendix, Fig. S3F and G*). To follow the dynamics of tension in real time, we used the molecular probe Flipper-TR (fluorescent lipid tension reporter [FlipTR]) that reports changes of membrane tension through changes of its fluorescence lifetime (Fig. 1*E*) (31, 39). Consistent with tube pulling experiments, the lifetime distribution of Flipper-TR in cell membranes before shock was broad: 4.76 ± 0.15 ns (Fig. 1*F*), and the lifetime changed within seconds after shock (Fig. 1*E and F*). We observed an asymmetry in lifetime measurements during recovery similar to the one observed for volume measurements: Membrane tension peaked and recovered within seconds after hypotonic shock while it decreased within seconds after hypertonic shock and continued decreasing for the duration of the experiment, although at a lower rate (Fig. 1*F*). Our results show that membrane tension variations after osmotic shocks qualitatively follow cell volume changes. To further investigate possible differences between volume and tension recovery, we studied them for 2 h after a mild hypertonic shock (600 mOsm). Cell volume slowly started recovering 15 min after the shock (*SI Appendix, Fig. S4A*). Consistent with refs. 40 and 41, recovery was still incomplete 2 h after the shock. Membrane tension had very different recovery dynamics: It started recovering only 50 min after the shock, but the recovery is fast and complete after 80 min (*SI Appendix, Fig. S4B*). These observations show that volume and tension responses after hypertonic shocks can be decoupled in the long term. This uncoupling may be due to reactivation of active cell processes, such as endocytosis or lipid metabolism, which may be triggered by a genetic response to the osmotic shock. Indeed, by reintroducing solutions with physiological osmolarities (315, 250, and 160 mOsm) at the time when volume recovery had started, but not tension recovery (20 min after shock; *SI Appendix, Fig. S4A and B*), we observed that volume and tension recoveries had the same dynamics (*SI Appendix, Fig. S4C–F*), but only hypotonic medium (160 mOsm) led to a full recovery (*SI Appendix, Fig. S4D*).

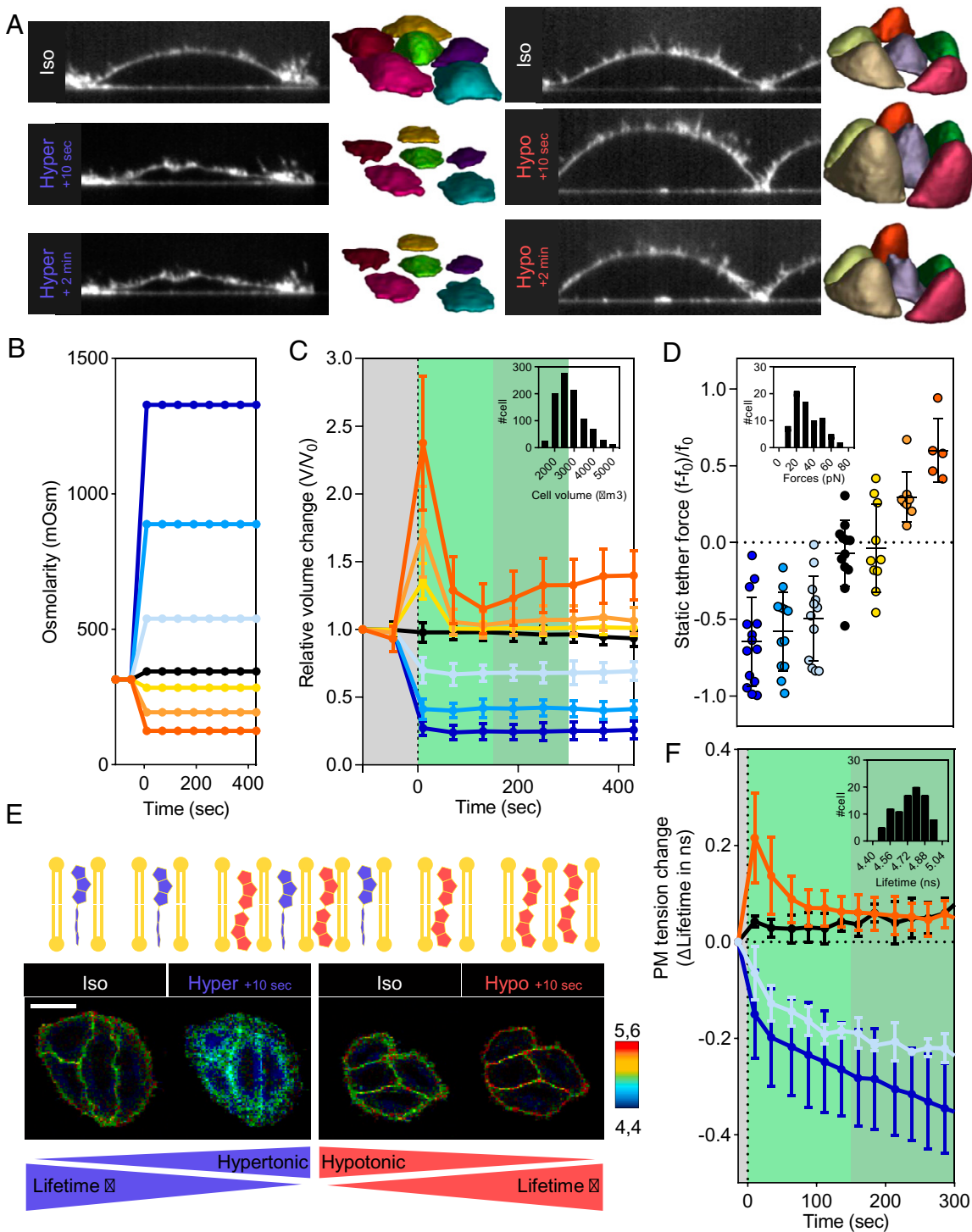


Fig. 1. Osmotic shocks affect cell volume and membrane tension. (A) Representative side view of cell with CellMask staining and corresponding 3D reconstruction of cell volume using Limeseg (Left, hyperosmotic; Right, hypoosmotic). (B) Osmolarities (mOsm) of cell media with time for the different stepwise osmotic conditions. Osmotic conditions correspond to 120 mOsm in dark orange, 190 mOsm in light orange, 285 mOsm in yellow, 315 mOsm in black, 540 mOsm in light blue, 890 mOsm in medium blue, and 1,330 mOsm in dark blue. Color code is maintained. (C) Averaged cell volume dynamics under osmotic shock (gray, before shocks; light green, short-term response; dark green, long-term response). Statistics are as follows: dark orange, $R > 3$, $n = 28$; light orange, $R > 3$, $n = 20$; yellow, $R > 3$, $n = 40$; black, $R > 3$, $n = 66$; light blue, $R > 3$, $n = 62$; medium blue, $R > 3$, $n = 47$; and dark blue, $R > 3$, $n = 43$. Inset shows cell volume distribution in isotonic medium before osmotic shocks ($R > 50$, $n = 959$). (D) Relative change of tether force immediately after osmotic shocks (averaged over 10 s) for different osmotic shocks. Inset shows tether force distribution in isotonic medium before osmotic shocks ($R = n = 73$). (E) Fluorescence lifetime of the Flipper-TR probe reports membrane tension changes. Shown are FLIM images of Flipper-TR lifetime values (color scale) of cells subjected to osmotic shocks. (F) Dynamics of the change of tension as measured by Flipper-TR lifetime (gray, before shock; light green, short-term response; dark green, long-term response). Osmotic conditions correspond to 120 mOsm in dark orange ($R = 7$, $n > 28$), 315 mOsm in black ($R = 3$, $n > 12$), 600 mOsm in light blue ($R = 3$, $n > 12$), and 1,330 mOsm in dark blue ($R = 5$, $n > 20$). Inset shows distribution of the cell average Flipper-TR lifetimes in isotonic medium before osmotic shocks ($R > 100$, $n > 400$).

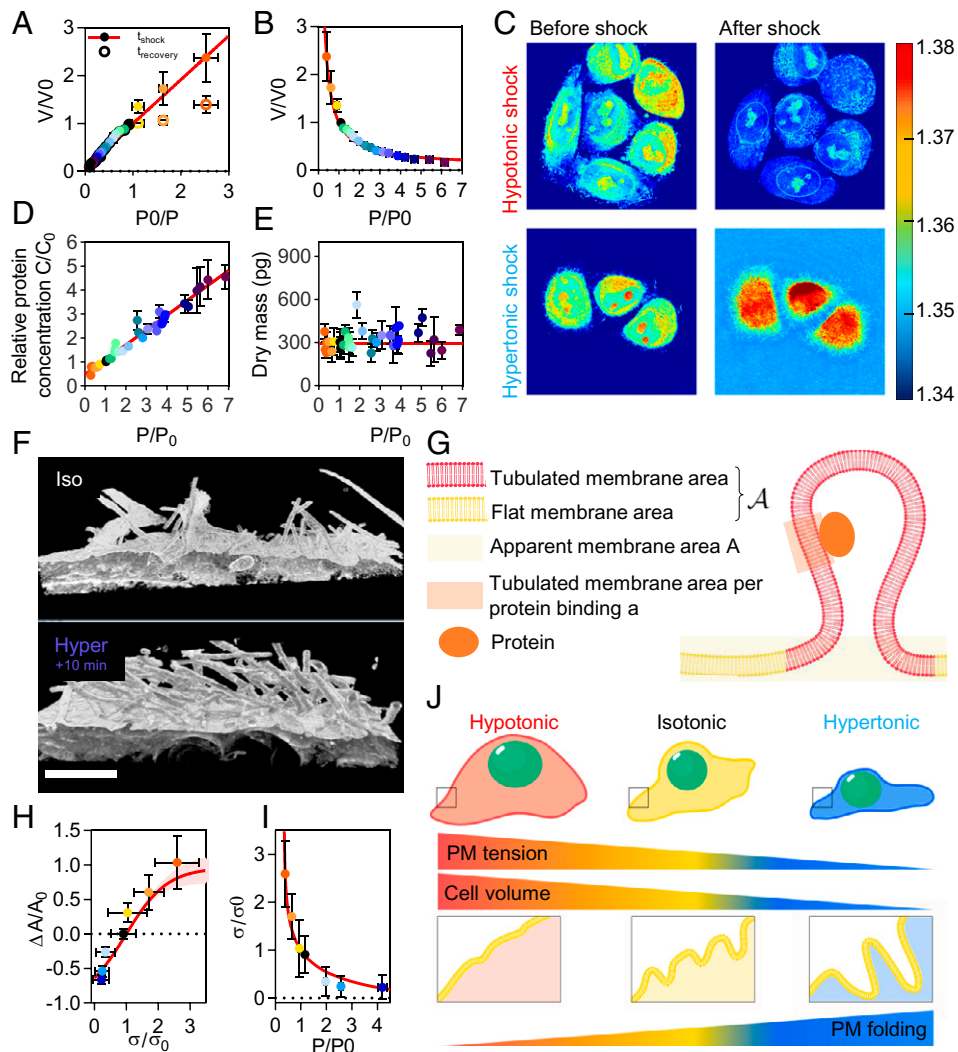


Fig. 2. Quantitative coupling of cell volume and cell membrane tension to osmotic shocks. (A) Normalized volume changes (V/V_0) as a function of osmotic pressure ratio (P_0/P) just after osmotic shocks (solid circle) and 8 min after the osmotic shock (open circle, recovery phase) compared to the prediction of Eq. 1 (red line). Color code is maintained from Fig. 1. Statistics are ($R > 3$, $n = 28$) for dark orange, ($R > 3$, $n = 20$) for light orange, ($R > 3$, $n = 40$) for yellow, ($R > 3$, $n = 66$) for black, ($R > 3$, $n = 62$) for light blue, ($R > 3$, $n = 47$) for medium blue, and ($R > 3$, $n = 43$) for dark blue. (B) Normalized volume changes (V/V_0) as a function of osmotic pressure ratio (P/P_0) just after osmotic shocks compared to the prediction of Eq. 1 (red line). Statistics are the same as in A. (C) Refractive index images of cells under osmotic shocks. (D) Protein concentration changes (C/C_0) according to pressure applied (P/P_0). Each point corresponds to one experiment containing at least two cells. Analysis is performed on individual cells. (E) Calculated dry mass of cells versus normalized pressure (P/P_0). Each point corresponds to one experiment containing at least two cells. Analysis is performed on individual cells. (F) Representative FIB-SEM images of the membrane tubulations in isotonic medium and hypertonic medium. (Scale bar: 2 μm .) (G) Scheme describing the parameters of the theory. (H) Relative changes of membrane area ($\Delta A/A_0$) versus relative changes of membrane tension ($\Delta\sigma/\sigma_0$) compared to the prediction of Eq. 3 (red line). Color code is maintained from Fig. 1. Statistics are ($R = n = 5$ in x ; $R > 3$, $n = 28$ in y) for dark orange, ($R = n = 8$ in x ; $R > 3$, $n = 20$ in y) for light orange, ($R = n = 10$ in x ; $R > 3$, $n = 40$ in y) for yellow, ($R = n = 12$ in x ; $R > 3$, $n = 66$ in y) for black, ($R = n = 12$ in x ; $R > 3$, $n = 62$ in y) for light blue, ($R = n = 12$ in x ; $R > 3$, $n = 47$ in y) for medium blue, and ($R = n = 14$ in x ; $R > 3$, $n = 43$ in y) for dark blue. (I) Normalized tension (σ/σ_0) versus normalized pressure (P/P_0) and prediction obtained using Eq. 4. Statistics are the same as in F. (J) Scheme describing the theory.

Altogether, these results support the notion that the coupling between cell volume and tension responses to osmotic shocks is kept at least 20 min after the shock.

Quantitative Coupling of Cell Volume to Osmotic Shocks. To quantitatively capture the relationship between the osmotic pressure of the cell and its volume (Fig. 2 A and B and *SI Appendix*, Fig. S5 A and B), we used the PBVH equation of state (34, 42)

$$P(V - V_{\text{OI}}) = P_0(V_0 - V_{\text{OI}}), \quad [1]$$

where P is the osmotic pressure of the intracellular medium, V is the cell volume, and P_0 and V_0 are values of P and V under isotonic conditions. Eq. 1 assimilates the contents of the cell

into a solution of particles with steric repulsions and otherwise negligible interactions, with the sum of the particles excluding volumes equal to V_{OI} . The cell volume thus cannot be compressed below the “osmotically inactive volume” V_{OI} . Eq. 1 is in excellent agreement with both our hypertonic and hypotonic data (Fig. 2 A and B), when the volume is estimated at the time of hypotonic peak (10 s after the shock, shown in Fig. 1C and *SI Appendix*, Fig. S1F). Interestingly, during and after the recovery phase (> 10 s after shock) volume values diverged from this linear relation only in the hypotonic conditions, reflecting the asymmetry of the recovery (Fig. 2 A and B). A single-parameter fit yields $V_{\text{OI}} = 300 \mu\text{m}^3$ equal to about 10% of the initial cell volume, smaller than previous estimates (43). Using RT-DC values on HL-60/S4 cells at the peak, we also find a good agreement

with $V_{OI} = 680\mu\text{m}^3$, which is about 30% of its initial cell volume. This difference can be explained by the smaller range of osmotic pressure measured for HL-60/S4 (SI Appendix, Fig. S5B) or by the intrinsic overestimation of cell volumes in RT-DC. It could also be that HL-60/S4 cells may also have a larger osmotically inactive volume, as it is known to be cell type specific (36).

Estimating the Osmotically Inactive Cell Volume. Our verification of the PBVH relation yields two surprising results: First, we find that it holds for a very large range of osmotic pressures in HeLa cells, larger than previously tested. Second, the V_{OI} represents a smaller proportion of V_0 [only 10%, compared to values between 7 and 50% in other studies (36, 44, 45)]. As the V_{OI} is obtained from a linear fit, the range of data and the formula used for the fit can strongly change the V_{OI} . We tested this possibility by changing the range of data used for the fit and show that using smaller ranges always provides larger V_{OI} (Materials and Methods). One may argue that the larger range of osmotic shocks we used may artificially give lower values of V_{OI} . To have an independent estimate of the V_{OI} , we sought to measure the protein mass of the cell and compare the hydrated minimal volume of this mass to our V_{OI} values. For this, we used optical diffraction tomography, a 3D tomographic label-free technique, to measure the cell's refractive index (RI) (46), hence giving a direct access to changes of cell mass and protein concentration. Cells in isotonic conditions had an average RI = 1.37 ± 0.01 . A few seconds after a hypertonic shock (1,330 mOsm), cells had an increase in RI to $1.42v \pm 0.01$, while under a hypotonic shock (120 mOsm) the RI decreased to 1.35 ± 0.01 (Fig. 2C). RI increases linearly with increasing protein concentration (47). In our experiment, the RI of single cells changed proportionally to the applied osmotic pressure (SI Appendix, Fig. S5C). This implies that the protein concentration changes proportionally to the osmotic pressure (Fig. 2D), which is fully consistent with our finding that cell volume changes proportionally to the osmotic pressure (Fig. 2A–C). Extracting the concentration from the RI and knowing the average cell volumes allow for calculation of the dry mass for each osmotic condition (Fig. 2E). The average dry mass of single HeLa cells was 305 ± 98 pg (SI Appendix, Fig. S5D) and, as expected, is constant throughout all osmotic shocks (Fig. 2E). To directly measure changes of concentration for a single protein within the cytoplasm, we measured the relative change of fluorescence intensity of cells overexpressing cytosolic GFP over time. It also varied proportionally to the osmotic pressure (SI Appendix, Fig. S5E–G). Thus, no significant amounts of intracellular proteins were exchanged with the environment, in agreement with previous studies (26, 33). Our measurement of the dry mass (Fig. 2E) also enabled an estimation of the V_{OI} . Multiplying the average volume of hydrated proteins per unit of dry mass (0.73 mL/g) (48) by the dry mass, we found $V_{OI} = 223.34 \pm 71.88\mu\text{m}^3$, in agreement with our PBVH fit.

Quantitative Coupling of Membrane Tension to Volume Changes and Osmotic Pressure. As the cell volume changes, so do the tension and area of its membrane (Fig. 1D–F and SI Appendix, Fig. S3D–G). To compute the relation between these quantities, we reasoned that the cell membrane is not perfectly flat, but is instead partly folded into tubular protrusions called filopodia, induced by the action of polymerizing actin. Many other proteins participate in the formation of those membrane protrusions, in particular inverted BAR (I-BAR) domain proteins (49). While other structures than filopodia such as caveolae may contain substantial amounts of surface, in our cells, the largest part of the membrane is stored in filopodia structures as seen from focused ion beam–scanning electron microscopy (FIB-SEM) 3D images (Fig. 2F). Protrusions in hypertonic medium (800 mOsm) are longer and larger than protrusions in isotonic medium (Fig. 2F). To account for the resulting reduction in apparent membrane area, we use a simple

model inspired by ref. 50 (Fig. 2G). In the model, the membrane exists in either one of two states, tubulated or flat (Fig. 2F), and is at equilibrium with a chemical reservoir of proteins provided by the cell's cytoplasm. When a protein binds to the membrane, one of the tubular protrusions grows. The tubulated membrane area thus increases by a , and the untubulated area decreases by the same amount. Note that the same reasoning can be applied to spherical buds. The free energy of the system is reduced by the binding free energy μ of the protein and increased by σa equal to the amount of work that must be performed against the membrane tension σ to reduce the untubulated area. The free energy μ regroups the protein entropy loss upon binding and the protein interaction with the membrane as well as the elastic cost of curving a membrane area a into a tube. As each tube contains many proteins, we neglect their translational free energy as well as the energetic cost of curving the membrane at their tip and base. Denoting the total membrane area by \mathcal{A} , we can thus represent the membrane by a set of $N = \mathcal{A}/a$ independent patches of area a , each of which can be tubulated or untubulated. The free energy difference between the two states reads $\mu - \sigma a$, implying that the partition function of the membrane reads $Z(\sigma) = z^N$, where the single-patch partition function reads

$$z = 1 + e^{(\mu - \sigma a)/k_B T}, \quad [2]$$

where $k_B T$ is the thermal energy. Denoting the apparent membrane area by A , the tubulated area is given by $\mathcal{A} - A = -k_B T \partial \ln Z / \partial \sigma$, implying that

$$\frac{\Delta A}{A_0} = \frac{e^{\mu/k_B T}}{e^{\mu/k_B T} + e^{\sigma a/k_B T}} [e^{(\sigma - \sigma_0)a/k_B T} - 1]. \quad [3]$$

Setting the isotonic tension σ_0 to its measured mean $\sigma_0 = 1.2 \times 10^{-4} \text{ N} \cdot \text{m}^{-1}$, the fit of this prediction to the data (Fig. 2H) yields a membrane area per protein $a = 53 \text{ nm}^2$ and a binding free energy $\mu = 1.5 k_B T$, corresponding to a binding free energy per unit area $\mu/a = 0.12 \text{ mN/m}$. This value is in line with estimates obtained for several protein coats (51) and more generally for energies of molecular interactions with surfaces (52). For these parameter values, we estimate that the ratio of total membrane area to membrane area in the isotonic state is $e^{\mu/k_B T} + e^{\sigma_0 a/k_B T} \simeq 2.0$. To obtain a further indication of the confidence interval over our fitted values, we estimate the magnitude of the changes in the values of a and μ that lead to a noticeably worse fit of the experimental data (which we formally define as an $\simeq 20\%$ increase of the sum of square residuals). We find that such changes are of the order of 15% for a and 10% for μ . To relate the change in membrane tension with the applied osmotic pressure, we combine the membrane's tension-strain relation Eq. 3 with the PBVH equation of state Eq. 1 under the assumption that the cell undergoes an approximately homogeneous dilation (contraction) when subjected to a hypoosmotic (hyperosmotic) shock. The last assumption implies that the volume and area of the cell respectively scale like the cube and the square of its typical lateral dimension. This implies $(A/A_0)^{1/2} = (V/V_0)^{1/3}$, which we combine with Eqs. 1 and 3 to yield

$$\frac{P}{P_0} = \frac{1 - \frac{V_{OI}}{V_0}}{\left[\frac{1 + e^{(\mu - \sigma_0 a)/k_B T}}{e^{\mu/k_B T} + e^{\sigma_0 a/k_B T}} e^{\sigma a/k_B T} \right]^{3/2} - \frac{V_{OI}}{V_0}}. \quad [4]$$

Eq. 4 yields a prediction for the dependence of the membrane tension on osmotic pressure, which is in good agreement with our data (Fig. 2I). These results strongly support the notion that the short-term responses of cell volume and membrane tension are predominantly mechanical and thermodynamic and consist of a passive equalization of the inner and outer osmotic pressures accompanied by an unfolding of membrane ruffles (Fig. 2J). To

further investigate the role of membrane ruffles in cell osmotic response, we first studied the role of the cytoskeleton in the cell response to osmotic shocks.

Actin and Microtubule Dynamics during Cell Osmotic Response. As in our system, most of the protrusions involved in buffering area expansion seemed to be filopodia-like structures, we sought to test the role of cortical actin in the osmotic shock response. We first imaged the dynamics of the actin cortex during osmotic shocks using SiR-Actin. Upon hypotonic shock, we observed cell blebbing concomitant with cortical actin depolymerization (*SI Appendix, Fig. S6A*). Blebs then extended and merged into a large membrane dome (*SI Appendix, Fig. S6A*, side view). By quantifying cortical actin fluorescence, we observed a complete repolymerization of the cortex 4 min after the shock (*SI Appendix, Fig. S6B*), to a value higher than the initial value. Following a hypertonic shock, the actin cytoskeleton appeared more condensed, and its fluorescence intensity gradually increased with time (*SI Appendix, Fig. S6B*). We also followed the behavior of microtubules using SiR-Tubulin. After hypotonic shocks, microtubules also depolymerized and appeared more condensed after a hypertonic shock, but to a smaller extent than actin (*SI Appendix, Fig. S6C and D*). These results suggested that actin is strongly depolymerized by the unfolding of the membrane upon hypotonic shocks but then repolymerizes to a thicker cortex when cell volume has fully recovered.

Impact of Cytoskeleton Inhibition or Stabilization on Cell Osmotic Response. To test this hypothesis, we used latrunculin A to depolymerize the F-actin or jasplakinolide to stabilize it (*Fig. 3A*). We then followed the cell volume and tension changes with time and compared them to those in untreated cells. First, we observed that dimethyl sulfoxide (DMSO), the solvent of stock solutions for the drugs we used, reduced the peak of volume after hypotonic shocks without affecting the peak of tension in control experiments, because DMSO increased the osmolarity of hypotonic solutions (*Materials and Methods*). As described below, none of the drugs used affected the response to hypertonic shocks (*Fig. 3B and SI Appendix, Fig. S7A*), consistent with the hypertonic response being essentially passive. Similarly, both drugs had little effect on the initial peak in cell volume after hypotonic shock, consistent with the short-term response to hypotonicity being passive and with a previous report on nonadherent cells (38). However, latrunculin radically modified the later-time recovery compared to that in nontreated and jasplakinolide-treated cells. Indeed, the volume of latrunculin-treated cells partially recovered after the initial peak, but then diverged a few minutes after shock (*Fig. 3B*). By contrast, the volume of jasplakinolide-treated cells evolved similarly to that of nontreated cells (*Fig. 3B*), although over a shorter timescale. Interestingly, the tension dynamics of both latrunculin- and jasplakinolide-treated cells were completely decoupled from volume dynamics, as no peak, and thus no recovery, was observed (*Fig. 3C*). Depolymerizing actin led to smaller initial tension (11) and smaller cell volume (*SI Appendix, Fig. S7B*) inducing more membrane reservoir available, which could explain the absence of membrane tension increase upon hypotonic shock (*Fig. 3C*). Stabilization of the actin also led to no increase of membrane tension under hypotonic shocks; we hypothesized that actin stretches to counterbalance the tension instead of stretching the membrane. Thus, the actin cortex is a major regulator of the coupling between membrane tension and volume dynamics (*Fig. 3C*). Depolymerization of microtubules with nocodazole had limited effects on the volume dynamics after hypotonic shocks but also decoupled tension from volume changes, as no tension changes were observed (*Fig. 3B and C*). Conversely, stabilizing microtubules with taxol clearly affected the dynamics of volume changes, as its peak was significantly smaller than in nontreated cells, and no recovery was observed. The smaller volume increase of taxol-treated cells

has also been observed in nonadherent cells (38) and could be due to the higher initial volume, which would reduce the size of membrane area buffer (*SI Appendix, Fig. S7B*). Maybe because of this lower area buffer, taxol-treated cells have a higher tension (11) and a stiffer membrane (53), which may explain why cell volume cannot recover after its further moderate increase (*Fig. 3B*). On the other hand, nocodazole-treated cells are softer (53) and have a lower initial volume (*SI Appendix, Fig. S7B*), which could be associated with a larger membrane area buffer. Consistent with this, and as seen for cells treated with latrunculin, tension does not change upon hypotonic shock in nocodazole-treated cells (*Fig. 3C*). These results show that tension dynamics can be decoupled from volume dynamics when actin and microtubule turnover is affected. As seen for taxol-treated cells, it is possible to qualitatively change the volume and tension response to osmotic shock, while preserving their coupling. Finally, none of the treatments affected the hypertonic response, supporting further that cells respond passively to this condition or at least without the involvement of the cytoskeleton (*SI Appendix, Fig. S7C*). While these results clearly show that the cytoskeleton is an essential actor in the cell response to osmotic shocks, several questions remained. Since actin was depolymerized during most of the recovery after hypotonic shocks, how is this recovery achieved? Also, the tight coupling between volume and tension responses suggests that it is under the control of a signaling pathway. In particular, we wondered what could be the role of caveolae, described as membrane tension buffering structures (6) and mTOR, a master signaling kinase involved in controlling membrane tension and membrane folding (7, 24).

Impact of Cavin1-Knockout on Cell Osmotic Response. We tested the role of caveolae in cell osmotic response by using HeLa Cavin1-KO, in which we fully invalidated the expression of the essential component of caveolae Cavin1 (*Fig. 4A and SI Appendix, Method*). In these cells, we observed that maximal cell volume increase under hypotonic shock corresponds to $1.5 * V_0$, similar to that for control cells transfected with CRISPR Cas-9 without guide RNA (called CRISPR control in the following) (*Fig. 4B and SI Appendix, Fig. S7D*). On the other hand, membrane tension increase was significantly higher in Cavin1-KO cells than in CRISPR control cells (*Fig. 4C and SI Appendix, Fig. S7E*). Using the calibration of lifetime to membrane tension from HeLa cells (31), a difference of $\Delta\tau = 0.2$ ns in hypotonic shocks corresponds to a doubling of membrane tension. The relative volume and membrane tension changes under hypertonic shocks (600 mOsm) were the same between the CRISPR control and the Cavin1-KO and they were not different from the control. We interpreted these results as caused by a reduced membrane reservoir in Cavin1-KO cells, hypotonic shocks would rapidly unfold the membrane area buffer, limiting volume expansion and increasing tension massively. Our observations are consistent with caveolae accounting for a limited portion of tension buffering (6).

Role of mTORCs Activity during Cell Osmotic Response. The rapid recovery of cell volume and tension during hypotonic shocks shows that these parameters are tightly and actively regulated by the cell. We studied the role of mTORC1 and mTORC2 in this regulation by following their kinase activity through phosphorylation of p70 and Akt, respectively (*Fig. 4A*). mTORC2 was quickly activated under hypotonic shock, as previously shown (7) (*Fig. 4D and SI Appendix, Fig. S7F*). We further observed that mTORC2 was rapidly inhibited under hypertonic shock (*Fig. 4D*). On the contrary, mTORC1 activity remained constant under hypotonic shock and was inhibited under hypertonic shock (*Fig. 4D*) as seen before in ref. 54. The high phosphorylation of Akt found at 0.1 s (*Fig. 4D*) was not reproducibly observed and may come from the fact that these cells were undergoing osmotic shocks in cold buffer, required to block dephosphorylation.

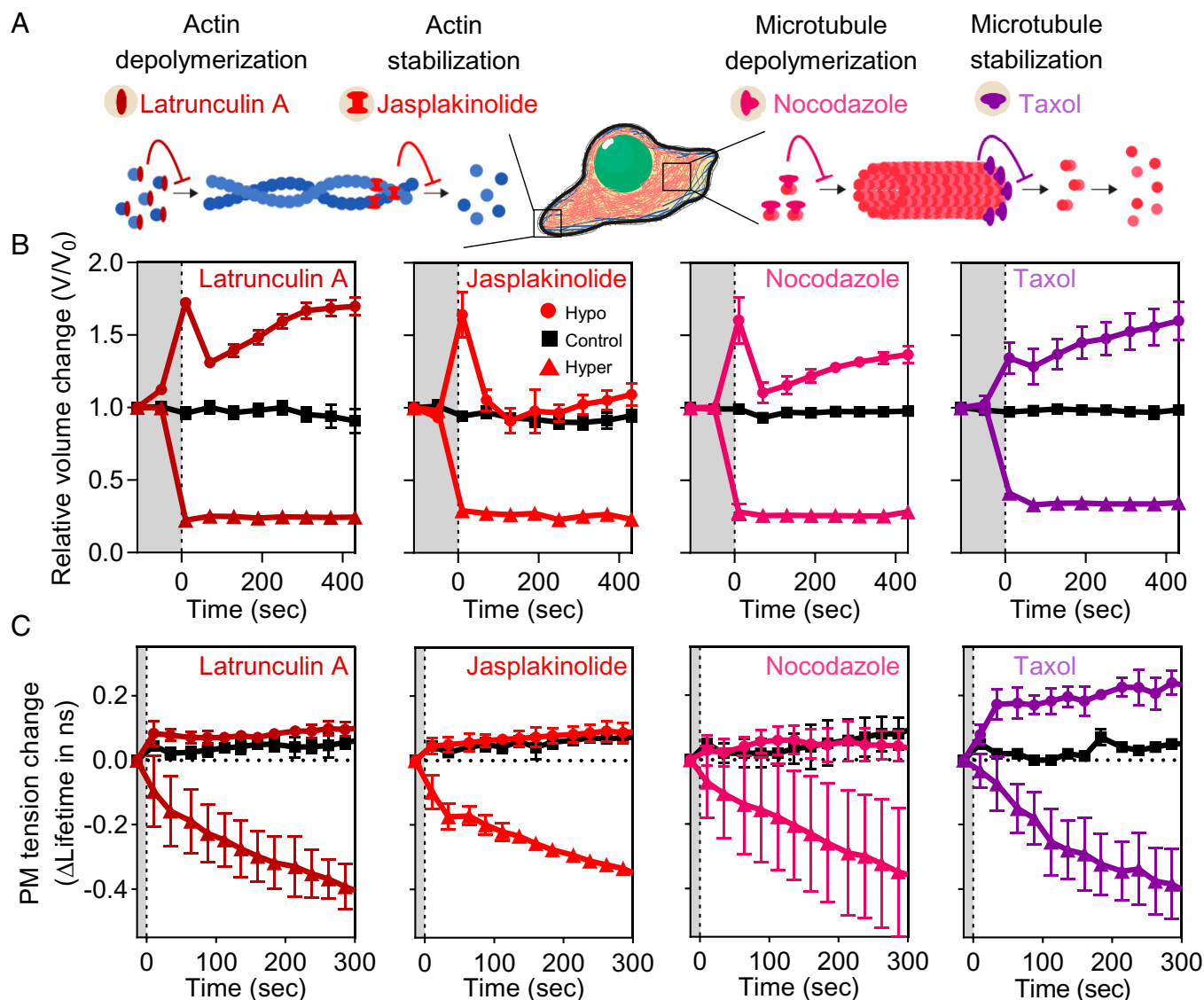


Fig. 3. Cytoskeleton controls the long-term response of cells to osmotic shocks. (A) Illustrations of cytoskeletal drug effects. (B) Single-cell volume dynamics of cells treated with latrunculin A, jasplakinolide, nocodazole, or taxol during hypotonic shocks (120 mOsm, circle), isotonic conditions (315 mOsm, square), and hypertonic shocks (700 mOsm; P/P0 = 2, triangle). Statistics are $R > 3$ for every experiment. For latrunculin A, $n = 5$ for control, $n = 4$ for hypo, $n = 15$ for hyper; for jasplakinolide, $n = 6$ for control, $n = 8$ for hypo, $n = 10$ for hyper; for nocodazole, $n = 8$ for control, $n = 8$ for hypo, $n = 6$ for hyper; for taxol, $n = 10$ for control, $n = 19$ for hypo, $n = 12$ for hyper. (C) Membrane tension dynamics of cells treated with latrunculin A, jasplakinolide, nocodazole, or taxol during the same shocks as in B. Statistics are $n > 4$ for every experiment. For latrunculin A, $R = 2$ for control, $R = 6$ for hypo, $R = 4$ for hyper; for jasplakinolide, $R = 4$ for control, $R = 10$ for hypo, $R = 3$ for hyper; for nocodazole, $R = 2$ for control, $R = 6$ for hypo, $R = 4$ for hyper; for taxol, $R = 2$ for control, $R = 3$ for hypo, $R = 4$ for hyper.

Unlike mTORC1, mTORC2 activation had similar dynamics under hypotonic and hypertonic shocks than volume and tension. This correlation suggested a more important role of mTORC2 than mTORC1 in regulating volume and tension response as well as their coupling. To test this hypothesis, we pharmacologically inhibited mTORCs and measured cell volume and tension responses under osmotic shocks. Both mTORC1 and mTORC2 are organized around the kinase mTOR, whose phosphorylation activity can be fully inhibited using Torin1, which thus inhibits both complexes (55) while rapamycin is a specific, partial inhibitor of mTORC1 (56) (Fig. 4A). First, we quantified the kinase activity of mTORC1 and mTORC2 following rapamycin and Torin1 treatment. We observed a complete inactivation of both complexes 30 min after Torin1 addition, while rapamycin fully inhibited p70 phosphorylation by mTORC1 after 20 min and without inhibiting mTORC2 (SI Appendix, Fig. S8A) in agreement with ref. 57. We then studied the effect of Torin1

and rapamycin treatments on the cell response to osmotic shocks. Volume changes induced by hypotonic shocks were only mildly affected by rapamycin, while Torin1-treated cells exhibited a significantly reduced volume peak after hypotonic shocks (Fig. 4E) when compared to nontreated cells. Rapamycin-treated cells also showed a peak of tension similar to that in nontreated cells followed by a slower recovery of tension. In Torin1-treated cells, a limited increase of tension, with no recovery, was observed (Fig. 4F). Both rapamycin- and Torin1-treated cells did not show significant changes of their volume and tension responses to hypertonic shock in comparison to nontreated cells (Figs. 1C and 4E and F and SI Appendix, Fig. S8B), strongly supporting that the cell response to hypertonic shock is essentially passive. These results suggest that mTORC2 controls the initial volume/tension coupling, while mTORC2 and mTORC1 are involved in the long-term recovery of both volume and tension. While mTORC complexes are

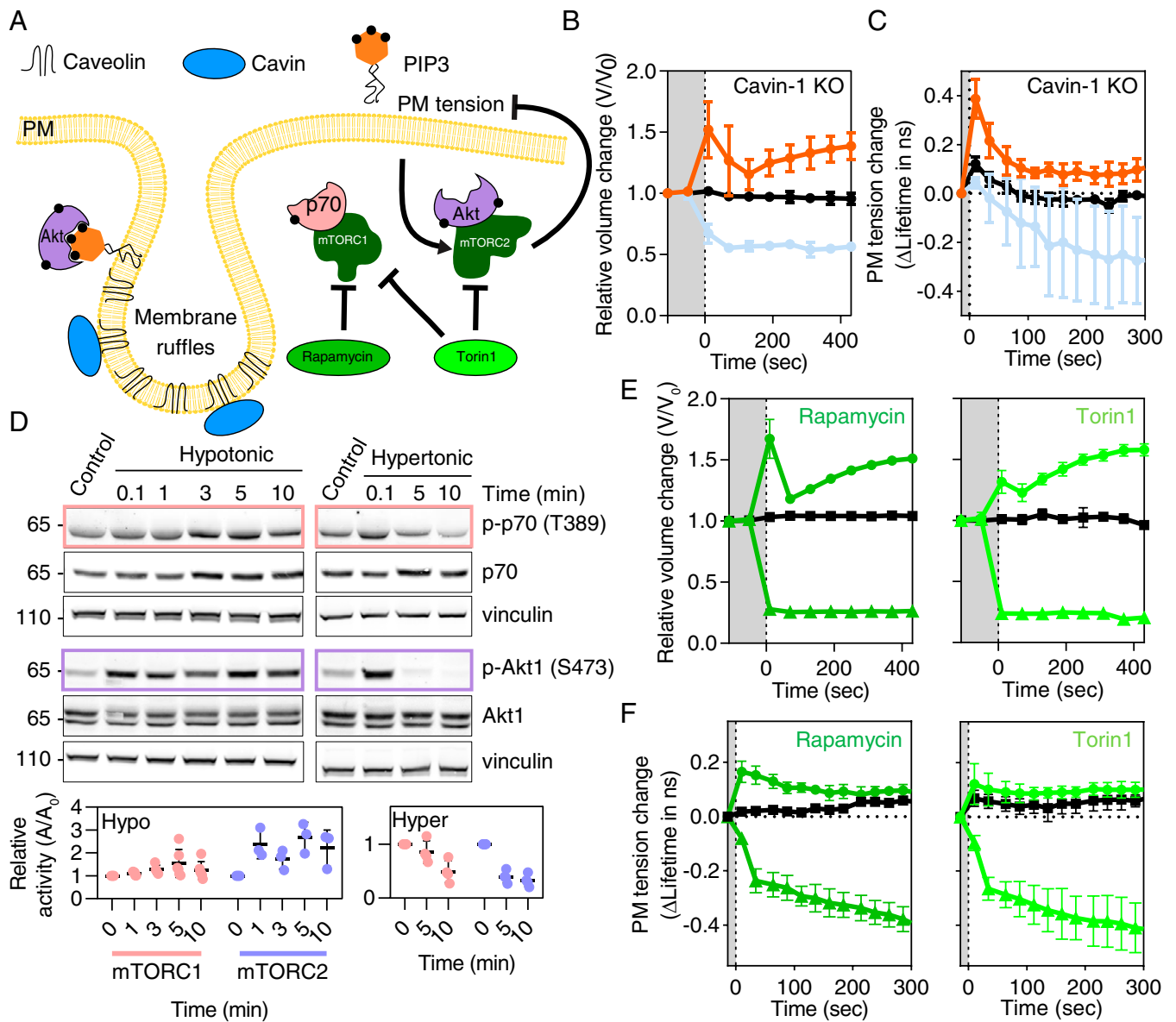


Fig. 4. Caveolae and mTORC2 are involved in membrane tension regulation. (A) Schematic of membrane ruffles interactions with caveolin1-2, cavin1-3, PIP3, and Akt phosphorylation as well as the signaling pathways of mTOR complexes inhibited by torin 1 (mTORC1 and mTORC2) or rapamycin (mTORC1). (B) Single-cell volume dynamics of cells Cav1-KO (and their corresponding CRISPR control; *SI Appendix, Fig. S7D*). Statistics are $R > 3$ for every experiment and $n = 7$ for control, $n = 15$ for hypo, $n = 18$ for hyper. (C) Membrane tension dynamics of cells Cav1-KO (and their corresponding CRISPR control; *SI Appendix, Fig. S7E*). Statistics are $n > 4$ for every experiment and $R = 3$ for control, $R = 4$ for hypo, $R = 2$ for hyper. (D) Activity of mTORC1 and mTORC2 under hypertonic and hypotonic shock. Panels represent activation (phosphorylation) of S6K1 (p-p70) and Akt (pAkt) and loading controls. Longer timepoints are in *SI Appendix, Fig. S7F* and corresponding quantification. (E) Single-cell volume dynamics of cells treated with rapamycin or Torin1 for hypotonic shocks (120 mOsm, circle), isotonic conditions (315 mOsm, square), and hypertonic shocks (700 mOsm; P/P0 = 2, triangle). Statistics are $R > 3$ for every experiment. For rapamycin, $n = 4$ for control, $n = 5$ for hypo, $n = 4$ for hyper; for Torin1, $n = 10$ for control, $n = 9$ for hypo, $n = 7$ for hyper. (F) Membrane tension dynamics of cells treated with rapamycin or Torin1 for identical shocks as in E. Statistics are $n > 4$ for every experiment. For rapamycin, $R = 2$ for control, $R = 6$ for hypo, $R = 4$ for hyper; for Torin1, $R = 7$ for control, $R = 15$ for hypo, $R = 4$ for hyper.

involved in the regulation of volume and tension responses to osmotic shocks and actin in the long-term recovery, factors involved in the initial, rapid recovery from hypotonic shocks remained unclear. Since actin was depolymerized during this phase, we postulated that ion transporters may be the primary actors of this fast recovery.

Role of Ion Transporters during Cell Osmotic Response. Exchangers and ion channels are essential regulators of cell volume. VRACs are involved in the cell response to osmotic shocks while NKCC1 and NHE participate in the osmotic balance of

cells in isotonic conditions. Furthermore, NHE1 and NKCC1 are interacting with F-actin (58, 59) and mTORCs (Fig. 5A) (24, 60) while VRAC has weak interactions with F-actin (61) and its link with mTORCs is still discussed (62, 63). We used pharmacological inhibitors of channels and transporters involved in osmotic stress response: the specific LRRC8A channel inhibitor 4-(2-butyl-6,7-dichloro-2-cyclopentylindan-1-on-5-yl)oxybutyric acid (DCPIB) inhibits VRACs, while 5-(*N*-ethyl-*N*-isopropyl)-Amiloride (EIPA) inhibits NHE exchanger and bumetanide inhibits NKCC1 exchanger (Fig. 5A). After hypotonic shocks, we observed a gradual impact of drugs

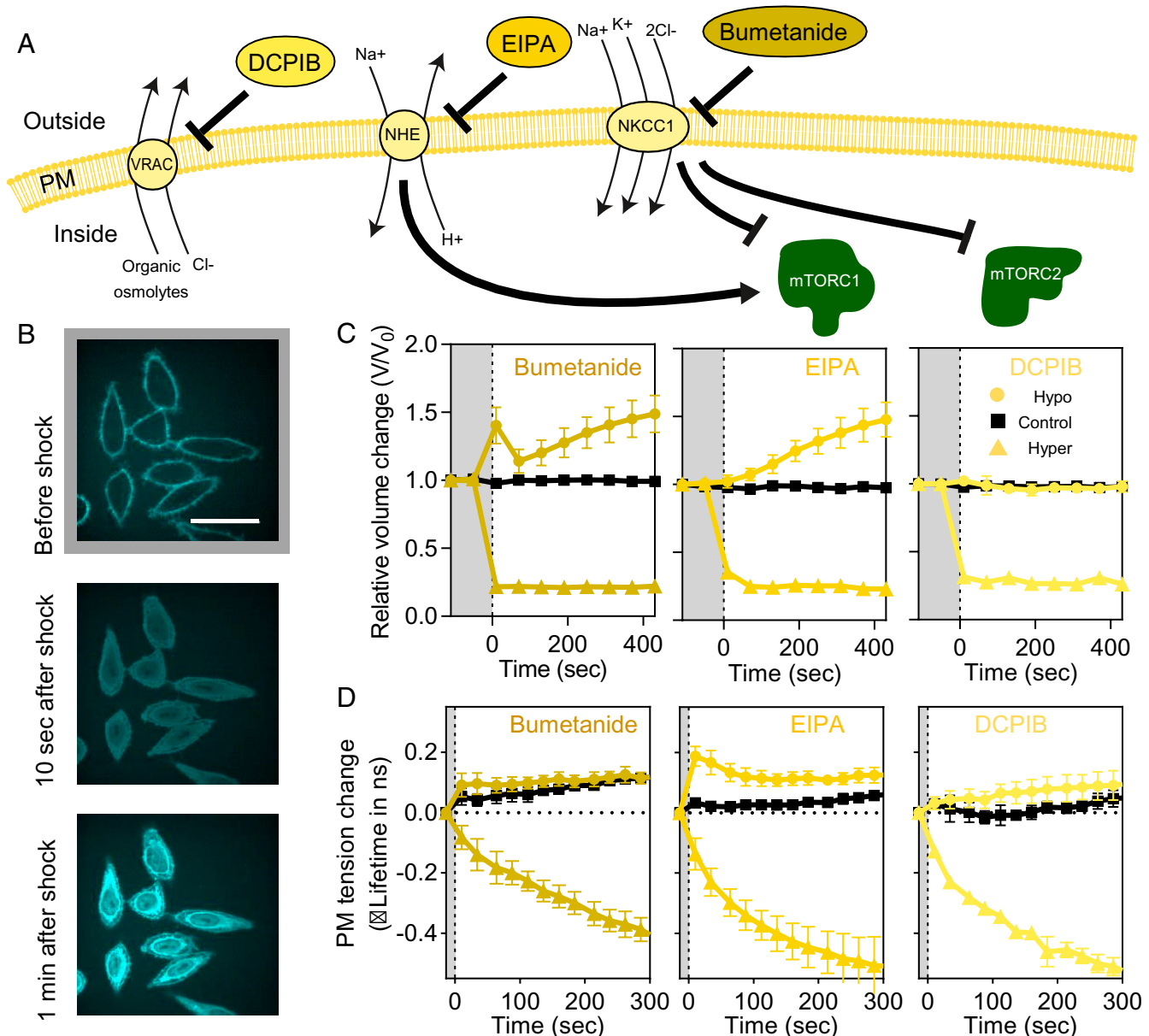


Fig. 5. Ion transporters are responsible for the short-term response of cells to osmotic shocks. (A) Illustrations of DCPIB, EIPA, and bumetanide pharmacological effects on, respectively, VRACs, NHE, and NKCC1 channels. (B) Confocal images of DCPIB-treated cells and response under hypotonic shock. (Scale bar: 40 μm .) (C) Single-cell volume dynamics in cells treated with bumetanide, EIPA, and DCPIB for hypotonic shocks (120 mOsm, circle), isotonic conditions (315 mOsm, square), and hypertonic shocks (700 mOsm; P/P0 = 2, triangle). Statistics are $R > 3$ for every experiment. For bumetanide, $n = 9$ for control, $n = 66$ for hypo, $n = 8$ for hyper; for EIPA, $n = 12$ for control, $n = 9$ for hypo, $n = 9$ for hyper; for DCPIB, $n = 12$ for control, $n = 31$ for hypo, $n = 14$ for hyper. (D) Membrane tension dynamics in cells treated with bumetanide, EIPA, and DCPIB for identical shocks as in C. Statistics are $n > 4$ for every experiment. For bumetanide, $R = 5$ for control, $R = 11$ for hypo, $R = 4$ for hyper; for EIPA, $R = 3$ for control, $R = 12$ for hypo, $R = 3$ for hyper; for DCPIB, $R = 2$ for control, $R = 6$ for hypo, $R = 2$ for hyper.

from bumetanide to DCPIB on the short-term cell swelling. DCPIB-treated cells were instantaneously permeabilized upon strong hypotonic shock, as seen by the instantaneous labeling of intracellular membranes with CellMask (120 mOsm, Fig. 5B). Cell volume did not change at all times in milder hypotonic conditions (25 and 50% water, Fig. 5C). By contrast, cells treated with bumetanide had a smaller but significant peak in cell volume (Fig. 5C), and EIPA-treated cells showed no peak immediately after hypotonic shock (Fig. 5C). In EIPA- and bumetanide-treated cells, cell volume slowly diverged 3 min after shock (Fig. 5C), consistent with the role of NHE and NKCC1 in slow volume homeostasis (18). All three drugs changed the tension response of cells to hypotonic shocks (Fig. 5D). For

bumetanide and EIPA, the response was clearly decoupled from the volume change but while EIPA-treated cells had a tension response equivalent to that in nontreated cells, in bumetanide-treated cells, tension did not significantly increase in comparison to the isotonic control and did not recover. Tension remained constant for DCPIB-treated cells, perfectly matching the volume dynamics, but this may be due to the rapid permeabilization of DCPIB-treated cells (Fig. 5B). In all hypertonic conditions, none of the inhibitors tested significantly affected the cell volume and tension responses, again indicating that the hypertonic response is essentially passive (Fig. 5C and D and *SI Appendix, Fig. S8C*). EIPA has no effect on adaptation from hypertonic shocks while EIPA is known to be an inhibitor of regulatory volume increases

(RVIs) because we are looking at a timescale when no volume increase had time to take place. Overall, these results show that ion transporters that participate in the osmotic balance of the cell also participate in the coupling between tension and volume changes during osmotic shocks and are primarily involved in the initial, large and rapid recovery from hypotonic shocks.

Discussion

Our study highlights the quantitative relation between cell volume changes and cell plasma membrane tension changes. We showed that cell volume changes are mainly due to cytoplasmic volume changes and confirm that cells modulate their volume according to the PBVH relation on a larger scale than previously reported (34). We observed two phases of cell volume response to osmotic shocks: the short-term response—a few seconds after the shock—which was characterized by cell volume variations according to the PBVH relation—and the second phase—a few tens of seconds to minutes after the shock—which we called the long-term response and was characterized by an asymmetric recovery. Indeed, cell volume recovered fast from hypotonic shocks, but recovered slowly from hypertonic shocks. By measuring cell volume and plasma membrane (PM) tension for 2 h after a mild hypertonic shock (600 mOsm), we observed that tension fully recovered, faster (30 min) than cell volume (70 min), which recovered only partially. Reactivation of endocytosis a few tens of minutes after the shock (64) might contribute to the faster tension recovery by removing excess membrane area. During those two phases, we observed that membrane tension changes followed cell volume changes. In the short-term response, evolution of tension with volume changes was consistent with a model based on membrane unfolding. Fits to the model yielded an estimate of the size of the membrane area buffer, i.e., the area stored in ruffles, about 1 to 1.5 times the projected area of the cell (maximal area being 2 to 2.5 times the initial projected area). It also gives a value of the binding free energy per unit area, which is of the same order as previous estimates (51). It also enabled inferring the change of tension according to the change of pressure applied outside the cells. This result is qualitatively maintained during the long-term response, as tension dynamically evolves with the same asymmetry as volume after hypotonic and hypertonic shocks. These results establish that tension passively follows volume changes during the entire duration of the response and recovery to osmotic shocks. One of the essential questions raised by the tight coupling of membrane tension and volume changes during osmotic shocks is, What are the determinants of this coupling? When we depleted caveolae, known to participate in buffering membrane tension, we observed a much higher increase of membrane tension under hypotonic shocks, consistent with ref. 6. Cell volume changes, on the other hand, were more limited than in parental cells, supporting the idea that depleting caveolae therefore removes membrane area buffer, limiting the expansion of cells during osmotic shocks. These results led to the notion that the membrane area buffer is a critical determinant of the coupling between cell volume and membrane tension. In further support of this notion, an inhibitor of the mTOR pathways decoupled tension and volume responses in the long-term response, consistent with the fact that mTORC1 is proposed to regulate cell volume homeostasis, while mTORC2 is proposed to regulate cell surface homeostasis (22). In the short-term response, only the inhibition of mTORC2 led to a reduced volume change while the tension mildly increased and did not recover. Durable mTORC2 inhibition by Torin1 in isotonic medium (*SI Appendix, Fig. S9A*) did not lead to PM tension change but cell volume is smaller (*SI Appendix, Fig. S9B*). PM tension increase during hypotonic shocks is limited, suggesting that cells have a high membrane area buffer (Figs. 4*F* and 6*A* and *SI Appendix, Fig. S9B*). Consistently, a similar response is found

when inhibiting NKCC1, which inhibits mTORC2 (24). mTORC2 might be the primary signaling complex coupling cell volume to tension due to its link to caveolae. Indeed, studies highlight a signaling pathway between caveolae and mTORC2 in mammals (7) similar to that between eisosomes and TORC2 in yeast (25), suggesting a common mechanism of membrane tension regulation. In mammals, PLD2 interacts with components of membrane invaginations (clathrin-coated pits and caveolae) and the mTORC2 complex (7), similar to that in Slm1 shuttles between eisosomes and TORC2, to inhibit its activity when tension increases (27). The feedback loops as mTORC2 regulates the dynamics of caveolin-1 phosphorylation (65) but the link between caveolae and Akt phosphorylation is under debate (66). Further evidence that the membrane area buffer directly affected the coupling between tension and volume came from studying downstream effectors of mTORC2 and notably the cytoskeleton. When microtubules were stabilized, the volume of cells increased (*SI Appendix, Fig. S7B*) as well as the osmotically inactive volume (*SI Appendix, Fig. S9C*). As a consequence, during hypotonic shocks, further volume increase was smaller, as well as tension, which did not recover (Fig. 3 *B* and *C*). These results are compatible with the notion that increased initial volume would reduce the membrane area buffer, limiting further changes (Fig. 6*A*). But even if the overall response was changed, the coupling between tension and volume change was preserved (Figs. 3 *B* and *C* and 6*B*). Altogether, these results support the hypothesis of regulations of cell volume and tension independent from the regulation of their coupling. A similar volume response to that in taxol-treated cells was obtained with EIPA, as it completely abrogated the initial volume increase under hypotonic shock. It is surprising since EIPA is known as an inhibitor of RVIs mostly tested in the context of mitosis (67) or adherence (68) but, to our knowledge, cell volume dynamics of EIPA-treated cells undergoing hypotonic shocks have never been tested before. As seen for taxol-treated cells, EIPA-treated cells have larger cell volume in isotonic medium (68) (*SI Appendix, Fig. S9B*) and a larger osmotically inactive volume (*SI Appendix, Fig. S9D*), again supporting the notion that increase in initial volume limits further increase upon hypotonic shocks. Again, these results support the idea that higher initial volume reduces the membrane area buffer (*SI Appendix, Fig. S9B*), limiting further changes of volume and tension during osmotic shocks. Consistently, cells with a smaller initial volume, treated with latrunculin A, jasplakinolide, or nocodazole (*SI Appendix, Fig. S7B*), undergo swelling under hypotonic shock without increase of their PM tension (Fig. 3 *B* and *C*). This is probably because their membrane area buffer is increased (Fig. 6*C*). Overall, our results support the notion that a large excess of membrane is stored in ruffles maintained by the cytoskeleton and that this area buffer sets the coupling of cell volume and membrane tension changes during osmotic shocks (*SI Appendix, Fig. S10*). The recovery phase is required to restore this large excess. Any initial modification of this membrane excess will impact the coupling of cell membrane tension and volume. When the cell volume dramatically increases because of hypotonicity, the cell initially responds by depolymerizing the cytoskeleton to drive membrane unfolding, which results in a release of membrane surface area. The initial volume recovery is mediated through ion transporters, as the cytoskeleton is still disrupted, and finalized with actin repolymerization to refold the membrane, under the control of mTOR signaling. Our results show that the coupling between tension and volume is actively regulated by the cytoskeleton, ion transporters, and mTOR signaling to maintain a quantitative relation between volume and tension well described by passive physical mechanisms. This coupling is regulated by the excess membrane buffer and is thus partially independent of specific regulatory mechanisms of tension and volume.

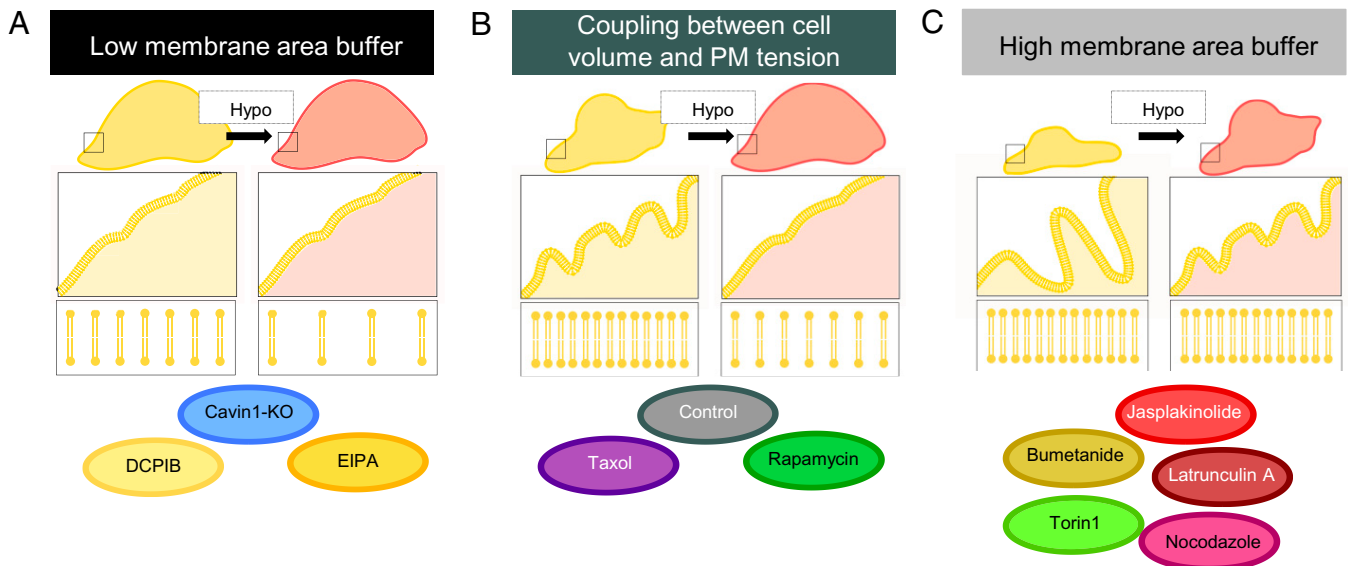


Fig. 6. Recapitulative scheme. (A) In the case of low membrane area buffer, cells have larger initial volumes that remain mostly unchanged during hypotonic shocks. Membrane ruffles are initially unfolded, which leads to higher stretching of the membrane and an increase of PM tension in resting conditions. (B) In the case of intermediate membrane area buffer, cell volumes increase under hypotonic shocks causing the unfolding of membrane ruffles. Membrane stretches and PM tension increases in a cell volume-dependent manner. (C) In the case of high membrane area buffer, cells have smaller initial volume, thus having also more ruffles and therefore cell volume increase under hypotonic shocks. Cell volume increase during hypotonic shock is responsible for unfolding the ruffles without stretching the membrane to its maximum, therefore having limited increase of PM tension.

Materials and Methods

A more detailed method is available in *SI Appendix*.

Cell Culture. HeLa-Kyoto and HeLa Kyoto EGFP-LaminB1/H2B-mCherry cells from Cell Lines Service (CLS) (330919) were cultured in Dulbecco's modified Eagle medium (DMEM), 4.5 g/L glucose. HL-60/S4 cells (American Type Culture Collection [ATCC] no. CRL-3306) were cultured in Gibco Roswell Park Memorial Institute (RPMI) medium (ATCC modification). The HeLa ATCC Cavin1-KO cell line and corresponding control were cultured in DMEM, 4.5 g/L glucose supplemented in pyruvate (see *SI Appendix, Method* about the cell line generation). All cell media were supplemented with 10% fetal bovine serum (10270-106; Thermofischer) and 1% penicillin-streptomycin in a 5% CO₂ incubator. Cells were authenticated by Microsynth and are mycoplasma negative, as tested by GATC Biotech, and are not on the list of commonly misidentified cell lines maintained by the International Cell Line Authentication Committee.

Image Acquisition and Analysis for Flipper-TR Imaging. Membrane tension measurements were performed on the setup published in ref. 31. HeLa Kyoto cells were labeled with Flipper-TR (Spirochrome SC020) in Leibovitz medium. Flipper-TR was dissolved in DMSO at 1 mM stock solutions. Cells were labeled with a 1:1,000 dilution from the DMSO stock and incubated at 37 °C for 15 min, and slices were acquired every 25 s for 10 min without washing the probe. Osmotic shocks were applied 10 s before the second timepoint. Lifetimes of Flipper-TR were extracted from fluorescence lifetime microscopy (FLIM) images using SymPhoTime 64 software (PicoQuant) with the same method published in ref. 31. We selected full images instead of choosing a region of interest.

1. A. L. Le Roux, X. Quiroga, N. Walani, M. Arroyo, P. Roca-Cusachs, The plasma membrane as a mechanochemical transducer. *Philos. Trans. R. Soc. Lond. B Biol. Sci.* **374**, 20180221 (2019).
2. J. A. Nichol, O. F. Hutter, Tensile strength and dilatational elasticity of giant sarcolemmal vesicles shed from rabbit muscle. *J. Physiol.* **493**, 187–198 (1996).
3. N. Groulx, F. Boudreault, S. N. Orlov, R. Grygorczyk, Membrane reserves and hypotonic cell swelling. *J. Membr. Biol.* **214**, 43–56 (2006).
4. E. Sitarska, A. Diz-Muñoz, Pay attention to membrane tension: Mechanobiology of the cell surface. *Curr. Opin. Cell Biol.* **66**, 11–18 (2020).
5. S. F. Pedersen, E. K. Hoffmann, J. W. Mills, The cytoskeleton and cell volume regulation. *Comp. Biochem. Physiol. A Mol. Integr. Physiol.* **130**, 385–399 (2001).
6. B. Sinha *et al.*, Cells respond to mechanical stress by rapid disassembly of caveolae. *Cell* **144**, 402–413 (2011).
7. A. Diz-Muñoz *et al.*, Membrane tension acts through PLD2 and mTORC2 to limit actin network assembly during neutrophil migration. *PLoS Biol.* **14**, e1002474 (2016).

Drug Treatment. Concentrations of drugs were kept constant throughout the experiment. Cells were preincubated in DMEM with drugs at 37 °C (see below for drug concentrations and incubation time). DMEM was replaced by Leibovitz with drugs and CellMask or Flipper-TR. The osmotic shocks were applied as before except that the solution contained the same drug concentration. The following pharmacological inhibitors were preincubated as follows: 50 nM latrunculin A for 1 h (Sigma L5163), 200 nM jasplakinolide for 30 min (Enzo ALX-350-275), 5 μM nocodazole for 30 min (Sigma M1404), 1 μM taxol for 1h (Sigma T1912), 100 μM DCPIB for 30 min (Tocris 1540), 50 μM EIPA for 30 min (Tocris 3378), 100 μM bumetanide for 30 min (Sigma B3023), 250 nM Torin1 for 30 min (LC Laboratories T-7887), and 100 nM rapamycin for 30 min (LC Laboratories R-5000). All the drugs were diluted in DMSO.

Data Availability. All study data are available at the following DOI: <https://doi.org/10.26037/yareta:izima5dpngngwne6zwoivrz67i>. Code are available on GitHub, <https://github.com/ChloeRoffay/3D-segmentation-time-tracking>.

ACKNOWLEDGMENTS. We thank K. Roux and R. Wimbish for critical reading of the manuscript and C. Tomba for discussions. A.R. acknowledges funding from Human Frontier Science Program Young Investigator Grant RGY0076/2009-C, Swiss National Fund for Research Grants 31003A_149975 and 31003A_173087, Synergia Grant CRSII5_189996, European Research Council Consolidator Grant 311536, and Synergia Grant 951324-R2-TENSION. This work has been supported by Institut Pasteur, CNRS, and ANR (SeptScort) (A.E.). V.A. received a fellowship from the Doctoral School Complexité du Vivant ED515 and La Ligue Contre le Cancer. M.L. was supported by ANR Grant ANR-15-CE13-0004-03 and European Research Council Starting Grant 677532. M.L.'s group belongs to the CNRS consortium Approches Quantitatives du Vivant.

8. L. Pan *et al.*, Hypotonic stress induces fast, reversible degradation of the vimentin cytoskeleton via intracellular calcium release. *Adv. Sci. (Weinh.)* **6**, 1900865 (2019).
9. J. Dai, M. P. Sheetz, X. Wan, C. E. Morris, Membrane tension in swelling and shrinking molluscan neurons. *J. Neurosci.* **18**, 6681–6692 (1998).
10. F. Guilak, G. R. Erickson, H. P. Ting-Beall, The effects of osmotic stress on the viscoelastic and physical properties of articular chondrocytes. *Biophys. J.* **82**, 720–727 (2002).
11. D. Raucher, M. P. Sheetz, Characteristics of a membrane reservoir buffering membrane tension. *Biophys. J.* **77**, 1992–2002 (1999).
12. P. G. Gillespie, R. G. Walker, Molecular basis of mechanosensory transduction. *Nature* **413**, 194–202 (2001).
13. O. P. Hamill, B. Martinac, Molecular basis of mechanotransduction in living cells. *Physiol. Rev.* **81**, 685–740 (2001).

14. D. Reeves, T. Ursell, P. Sens, J. Kondev, R. Phillips, Membrane mechanics as a probe of ion-channel gating mechanisms. *Phys. Rev. E Stat. Nonlin. Soft Matter Phys.* **78**, 041901 (2008).
15. B. Martinac, The ion channels to cytoskeleton connection as potential mechanism of mechanosensitivity. *Biochim. Biophys. Acta* **1838**, 682–691 (2014).
16. R. Syeda *et al.*, LRRRC8 proteins form volume-regulated anion channels that sense ionic strength. *Cell* **164**, 499–511 (2016).
17. T. J. Jentsch, VRACs and other ion channels and transporters in the regulation of cell volume and beyond. *Nat. Rev. Mol. Cell Biol.* **17**, 293–307 (2016).
18. E. K. Hoffmann, I. H. Lambert, S. F. Pedersen, Physiology of cell volume regulation in vertebrates. *Physiol. Rev.* **89**, 193–277 (2009).
19. A. Diz-Muñoz, D. A. Fletcher, O. D. Weiner, Use the force: Membrane tension as an organizer of cell shape and motility. *Trends Cell Biol.* **23**, 47–53 (2013).
20. S. Hohmann, Osmotic stress signaling and osmoadaptation in yeasts. *Microbiol. Mol. Biol. Rev.* **66**, 300–372 (2002).
21. K. Christoph, F. X. Beck, W. Neuhofer, Osmoadaptation of mammalian cells - an orchestrated network of protective genes. *Curr. Genomics* **8**, 209–218 (2007).
22. M. Riggi, B. Kusmider, R. Loewith, The flipside of the TOR coin—TORC2 and plasma membrane homeostasis at a glance. *J. Cell Sci.* **133**, jcs242040 (2020).
23. M. Delarue *et al.*, mTORC1 controls phase separation and the biophysical properties of the cytoplasm by tuning crowding. *Cell* **174**, 338–349.e20 (2018).
24. W. L. Demian *et al.*, The ion transporter NKCC1 links cell volume to cell mass regulation by suppressing mTORC1. *Cell Rep.* **27**, 1886–1896.e6 (2019).
25. M. Riggi *et al.*, Decrease in plasma membrane tension triggers PtdIns(4,5)P₂ phase separation to inactivate TORC2. *Nat. Cell Biol.* **20**, 1043–1051 (2018).
26. M. Riggi *et al.*, TORC2 controls endocytosis through plasma membrane tension. *J. Cell Biol.* **218**, 2265–2276 (2019).
27. D. Berchtold *et al.*, Plasma membrane stress induces relocalization of Slm proteins and activation of TORC2 to promote sphingolipid synthesis. *Nat. Cell Biol.* **14**, 542–547 (2012).
28. E. Jacinto *et al.*, Mammalian TOR complex 2 controls the actin cytoskeleton and is rapamycin insensitive. *Nat. Cell Biol.* **6**, 1122–1128 (2004).
29. A. Echarrí, M. A. Del Pozo, Caveolae - mechanosensitive membrane invaginations linked to actin filaments. *J. Cell Sci.* **128**, 2747–2758 (2015).
30. A. Pietuch, B. R. Brückner, A. Janshoff, Membrane tension homeostasis of epithelial cells through surface area regulation in response to osmotic stress. *Biochim. Biophys. Acta* **1833**, 712–722 (2013).
31. A. Colom *et al.*, A fluorescent membrane tension probe. *Nat. Chem.* **10**, 1118–1125 (2018).
32. M. A. A. Aye, E. LeMaster, T. Teng, J. Lee, I. Levitan, Hypotonic challenge of endothelial cells increases membrane stiffness with no effect on tether force. *Biophys. J.* **114**, 929–938 (2018).
33. S. Boulant, C. Kural, J. C. Zeeh, F. Ubelmann, T. Kirchhausen, Actin dynamics counteract membrane tension during clathrin-mediated endocytosis. *Nat. Cell Biol.* **13**, 1124–1131 (2011).
34. J. D. Finan, K. J. Chalut, A. Wax, F. Guilak, Nonlinear osmotic properties of the cell nucleus. *Ann. Biomed. Eng.* **37**, 477–491 (2009).
35. E. H. Zhou *et al.*, Universal behavior of the osmotically compressed cell and its analogy to the colloidal glass transition. *Proc. Natl. Acad. Sci. U.S.A.* **106**, 10632–10637 (2009).
36. I. I. Katkov, On proper linearization, construction and analysis of the Boyle-van't Hoff plots and correct calculation of the osmotically inactive volume. *Cryobiology* **62**, 232–241 (2011).
37. O. Otto *et al.*, Real-time deformability cytometry: On-the-fly cell mechanical phenotyping. *Nat. Methods* **12**, 199–202 (2015).
38. A. K. Fajrial *et al.*, Characterization of single-cell osmotic swelling dynamics for new physical biomarkers. *Anal. Chem.* **93**, 1317–1325 (2021).
39. M. Dal Molin *et al.*, Fluorescent flippers for mechanosensitive membrane probes. *J. Am. Chem. Soc.* **137**, 568–571 (2015).
40. M. Guo *et al.*, Cell volume change through water efflux impacts cell stiffness and stem cell fate. *Proc. Natl. Acad. Sci. U.S.A.* **114**, E8618–E8627 (2017).
41. S. A. Serra *et al.*, LRRRC8A-containing chloride channel is crucial for cell volume recovery and survival under hypertonic conditions. *Proc. Natl. Acad. Sci. U.S.A.* **118**, e2025013118 (2021).
42. E. Ponder, *Hemolysis and Related Phenomena* (Grune Stratton, New York, 1948).
43. Y. Xu *et al.*, A single-cell identification and capture chip for automatically and rapidly determining hydraulic permeability of cells. *Anal. Bioanal. Chem.* **412**, 4537–4548 (2020).
44. D. Peckys, P. Mazur, Regulatory volume decrease in COS-7 cells at 22 °C and its influence on the Boyle van't Hoff relation and the determination of the osmotically inactive volume. *Cryobiology* **65**, 74–78 (2012).
45. H. Shapiro, The change in osmotically inactive fraction produced by cell activation. *J. Gen. Physiol.* **32**, 43–51 (1948).
46. K. Kim, J. Guck, The relative densities of cytoplasm and nuclear compartments are robust against strong perturbation. *Biophys. J.* **119**, 1946–1957 (2020).
47. H. Zhao, P. H. Brown, P. Schuck, On the distribution of protein refractive index increments. *Biophys. J.* **100**, 2309–2317 (2011).
48. R. Schlüssler *et al.*, Mechanical mapping of spinal cord growth and repair in living zebrafish larvae by Brillouin imaging. *Biophys. J.* **115**, 911–923 (2018).
49. S. Guerrier *et al.*, The F-BAR domain of srGAP2 induces membrane protrusions required for neuronal migration and morphogenesis. *Cell* **138**, 990–1004 (2009).
50. I. Lavi *et al.*, Cellular blebs and membrane invaginations are coupled through membrane tension buffering. *Biophys. J.* **117**, 1485–1495 (2019).
51. M. Saleem *et al.*, A balance between membrane elasticity and polymerization energy sets the shape of spherical clathrin coats. *Nat. Commun.* **6**, 6249 (2015).
52. E. Evans, Probing the relation between force–lifetime—and chemistry in single molecular bonds. *Annu. Rev. Biophys. Biomol. Struct.* **30**, 105–128 (2001).
53. K. Mandal, A. Asnacios, B. Goud, J. B. Manneville, Mapping intracellular mechanics on micropatterned substrates. *Proc. Natl. Acad. Sci. U.S.A.* **113**, E7159–E7168 (2016).
54. M. Plescher, A. A. Teleman, C. Demetriades, TSC2 mediates hyperosmotic stress-induced inactivation of mTORC1. *Sci. Rep.* **5**, 13828 (2015).
55. Q. Liu *et al.*, Discovery of 1-(4-(4-propionylpiperazin-1-yl)-3-(trifluoromethyl)phenyl)-9-(quinolin-3-yl)benzo[h][1,6]naphthyridin-2(1H)-one as a highly potent, selective mammalian target of rapamycin (mTOR) inhibitor for the treatment of cancer. *J. Med. Chem.* **53**, 7146–7155 (2010).
56. F. Boutouja, C. M. Stiehm, H. W. Platta, mTOR: A cellular regulator interface in health and disease. *Cells* **8**, 18 (2019).
57. Y. Bai *et al.*, Differential role of rapamycin in epidermis-induced IL-15-IGF-1 secretion via activation of Akt/mTORC2. *Cell. Physiol. Biochem.* **42**, 1755–1768 (2017).
58. S. P. Denker, D. L. Barber, Ion transport proteins anchor and regulate the cytoskeleton. *Curr. Opin. Cell Biol.* **14**, 214–220 (2002).
59. C. M. Liedtke, M. Hubbard, X. Wang, Stability of actin cytoskeleton and PKC-delta binding to actin regulate NKCC1 function in airway epithelial cells. *Am. J. Physiol. Cell Physiol.* **284**, C487–C496 (2003).
60. M. E. Meima, B. A. Webb, H. E. Witkowska, D. L. Barber, The sodium-hydrogen exchanger NHE1 is an Akt substrate necessary for actin filament reorganization by growth factors. *J. Biol. Chem.* **284**, 26666–26675 (2009).
61. B. König, Y. Hao, S. Schwartz, A. J. Plested, T. Stauber, A FRET sensor of C-terminal movement reveals VRAC activation by plasma membrane DAG signaling rather than ionic strength. *eLife* **8**, e45421 (2019).
62. I. H. Lambert, J. V. Jensen, P. A. Pedersen, mTOR ensures increased release and reduced uptake of the organic osmolyte taurine under hyposmotic conditions in mouse fibroblasts. *Am. J. Physiol. Cell Physiol.* **306**, C1028–C1040 (2014).
63. A. Kumar *et al.*, SWELL1 regulates skeletal muscle cell size, intracellular signaling, adiposity and glucose metabolism. *eLife* **9**, e58941 (2020).
64. H. De Belly *et al.*, Membrane tension gates ERK-mediated regulation of pluripotent cell fate. *Cell Stem Cell* **28**, 273–284.e6 (2021).
65. A. M. Hau *et al.*, Dynamic regulation of Caveolin-1 phosphorylation and caveolae formation by mammalian target of rapamycin complex 2 in bladder cancer cells. *Am. J. Pathol.* **189**, 1846–1862 (2019).
66. M. G. Sugiyama, G. D. Fairn, C. N. Antonescu, Akt-ing up just about everywhere: Compartment-specific akt activation and function in receptor tyrosine kinase signaling. *Front. Cell Dev. Biol.* **7**, 70 (2019).
67. M. P. Stewart *et al.*, Hydrostatic pressure and the actomyosin cortex drive mitotic cell rounding. *Nature* **469**, 226–230 (2011).
68. K. Xie, Y. Yang, H. Jiang, Controlling cellular volume via mechanical and physical properties of substrate. *Biophys. J.* **114**, 675–687 (2018).